# Chapter 3
# Acquiring 4D Thoracic CT Scans Using Ciné CT Acquisition

**Daniel Low**

**Abstract** One method for acquiring 4D thoracic CT scans is to use ciné acquisition. Ciné acquisition is conducted by rotating the gantry and acquiring x-ray projections while keeping the couch stationary. After a complete rotation, a single set of CT slices, the number corresponding to the number of CT detector rows, is produced. The rotation period is typically sub second so each image set corresponds to a single point in time. The ciné image acquisition is repeated for at least one breathing cycle to acquire images throughout the breathing cycle. Once the images are acquired at a single couch position, the couch is moved to the abutting position and the acquisition is repeated. Post-processing of the images sets typically resorts the sets into breathing phases, stacking images from a specific phase to produce a thoracic CT scan at that phase. Benefits of the ciné acquisition protocol include, the ability to precisely identify the phase with respect to the acquired image, the ability to resort images after reconstruction, and the ability to acquire images over arbitrarily long times and for arbitrarily many images (within dose constraints).

## 3.1 Introduction

One of the uses of CT scan acquisition is to obtain images that can be used to model human breathing motion. CT scans are relatively fast; modern scanners can acquire images in less than 0.4 s, and around 0.2 s if fewer than 360° of projections are required. This speed reduces breathing motion artifacts that occur when scanner rotation periods are more than 1 s.

There are two basic modes of CT scanning. By far, the most common is helical CT (the subject of Chap. 2), whereby the CT scanner rotates as the couch moves with a uniform speed. The radiation beam central axis traces a helix through the patient

D. Low
UCLA Radiation Oncology, Los Angeles, CA, USA
e-mail: DLow@mednet.ucla.edu

J. Ehrhardt and C. Lorenz (eds.), *4D Modeling and Estimation of Respiratory Motion for Radiation Therapy*, Biological and Medical Physics, Biomedical Engineering,
DOI: 10.1007/978-3-642-36441-9_3, © Springer-Verlag Berlin Heidelberg 2013

as the projection data are acquired. This method is the most efficient method for acquiring CT data. The couch can be moved more than the width of the collimated beam during each rotation (pitch >1) which, when coupled with a fast rotation rate and large longitudinal coverage, makes helical scanning extremely fast; CT scans of the thorax can be acquired within two seconds with modern scanners.

The couch motion for helical scanning is typically constrained to be constant; once the parameters of pitch, field size, and rotation rate are selected, the couch speed is fixed. While this is not a problem for standard scanning, it provides a significant constraint for 4D imaging. In order to acquire useful breathing modeling data, CT data need to be acquired during at least one breath. Breathing periods are approximately 5 s, so the minimum time that any one region of tissue needs to be imaged is 5 s. While the CT scanner rotation rate can be slowed down to guarantee that each portion of the patient is being imaged for 5 s, such slow acquisition will lead to breathing motion artifacts. The CT scan rotation period needs to be less than 0.5 s to avoid these artifacts. Rather than slow rotation rate, most helical CT scanning protocols reduce the pitch, slowing the couch and acquiring multiple images at each location within the patient. The protocols are designed such that each portion of the patient is scanned for a period of at least 5 s [3, 7].

While helical scanning is the dominant acquisition mode and a 4D helical scanning solution has been found and implemented for most commercial systems, helical scanning has some significant limitations. First, the minimum pitch for CT scanners is approximately 0.15, which when combined with a rotation rate of 0.5 s, leads to a total amount of time that any one location is scanned of 0.5/0.06 s = 8.33 s. This amount of time is greater than the breathing period for most patients, which means that for most patients and most times, CT images will be scanned throughout the breathing cycle for the whole patient. Many patients have irregular breathing cycles and some take pauses in their breathing. The CT scanner cannot pause a helical CT acquisition, so image artifacts will occur if the patient breathing pauses for more than a few seconds. Figure 3.1 shows examples from Lu et al. [6] of breathing patterns that have such irregularities.

## 3.2 Benefits of Ciné CT

Ciné acquisition, in contrast to helical acquisition, is conducted with a stationary couch. The CT scanner rotates and acquires projection data over a longitudinal span that nearly matches the radiation field length. The length of this span depends on the detector layout and is usually between 2 and 4 cm (see Sect. 2.2.2). The number of acquisitions per couch position is programmed in advance and the CT rotation time determines the temporal resolution of the scan. The number of scans multiplied by the scan period is the minimum amount of time that scans can be acquired for, but pauses between scans can be programmed to lengthen the effective scan time to assure that at least one breathing period occurs at each couch position. In fact, the

amount of time can easily be stretched to multiple breathing periods to reduce the chance that no motion data are acquired because of breathing irregularities.

Ciné CT acquisition provides many benefits over helical acquisition. Principally, the number of scans is selectable and not constrained by couch speed limitations. Prospective gating is also possible with ciné-CT [4]. Ciné-CT protocols can be programmed to be started by an external trigger, set for example to specific phases of the breathing cycle. Sophisticated analysis of the breathing cycle could be conducted to assure that only images that will provide the required breathing motion data will be acquired, reducing the radiation dose to the patient and improving the usability of the CT scan data.

CT images are reconstructed using x-ray projections from up to 360°. In helical multislice CT, the projection angles also include an out-of-plane angle. Ideally these projections would be acquired over a limited period of time. In order to minimize image noise, however, when reconstructing an image at a specific breathing phase, manufacturers utilize each projection acquired during a time consistent with that breathing phase. The projections may therefore be acquired during different breaths. If the user wants to use the commercial sorting algorithm to reconstruct images, there is no problem, but if the user wants to control the specific timepoints from which projection data are taken, this process is not useful. An advantage of ciné CT is that the projections used to acquire the CT data are acquired only during the gantry rotation time for the specific ciné acquisition. This allows the user to precisely control the timepoints at which the data are acquired for subsequent reconstructions. Pat et al. [7] compared data sufficiency conditions for helical and ciné acquisitions using a 20 cm coverage, 4 s breathing cycle, half-scan reconstruction. He found that the helical acquisition benefited from more rapid scan time (by 10 %) than the ciné acquisition. The helical slice sensitivity profile was 1.8 times broader than the ciné profile and required an additional breathing cycle of scanning at the beginning and end of the scan to assure adequate sampling at the ends of the scans. The ciné scans also delivered between 4 and 8 % less dose than the helical acquisition.

Table 3.1 shows a summary of the comparison between helical and ciné acquisitions.

**Table 3.1** Summary of the comparison between helical and ciné acquisition

| | Ciné | Helical |
|---|---|---|
| Temporal resolution | ++ | + |
| Temporal control (knowing when image data were acquired) | ++ | – |
| Spatial resolution (blurring) | ++ | + |
| Ability to prospectively gate | ++ | – |
| Image artifacts | – | + |
| Ability to manage irregular breathing | + | – |
| Ability to do amplitude based sorting | ++ | ++ |
| Acquisition flexibility | ++ | – |
| Cone beam artifacts (assuming fan-beam ciné reconstruction) | – | ++ |

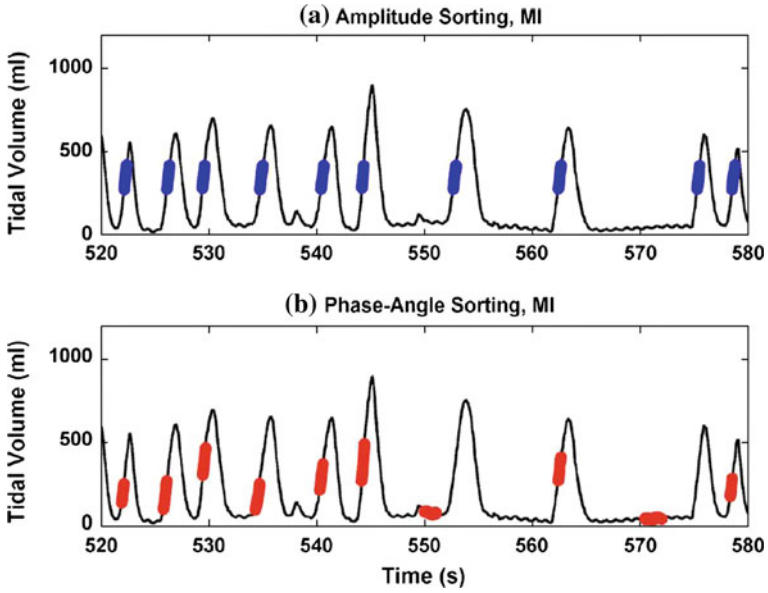


**Fig. 3.1** Example of irregular breathing waveforms highlighting that breathing patterns can pause for times approaching 10 s. Figure is from Lu et al. [6]

## 3.3 Development of Volumetric CT Using Ciné CT Scans

Ciné CT scan acquisition yields a series of CT slice scans (collections), each acquired at different times and breathing phases. Between 10 and 25 repeated CT scans are acquired per table position before the table is moved to the next position, and this process is repeated until the entire volume of interest is scanned. The process of generating useful 4D CT images that encompass the organs of interest involves the building of 3D CT images at different breathing phases using the acquired ciné images.

There are two current approaches to generate 4D CT images from ciné CT acquisitions and a breathing surrogate measured at acquisition time. They are termed amplitude-based sorting and phase-based sorting. Figure 3.2 shows an example of the amplitude-based process as described by Low et al. [5]. They selected the tidal volume measured with spirometry as the method for describing the breathing cycle. To create a 3D CT image at a specific tidal volume, they selected the ciné scans that were obtained at each couch position with a tidal volume closest to the desired volume. The result was a full 3D CT that represented the patient geometry as though the patient had been scanned at that tidal volume. This process could be repeated for any tidal volume for which there was sufficient scan data.

General Electric used a phase-based approach with their commercial ciné 4D CT scanners [8, 10]. Figure 3.3 shows the process that GE uses to acquire their

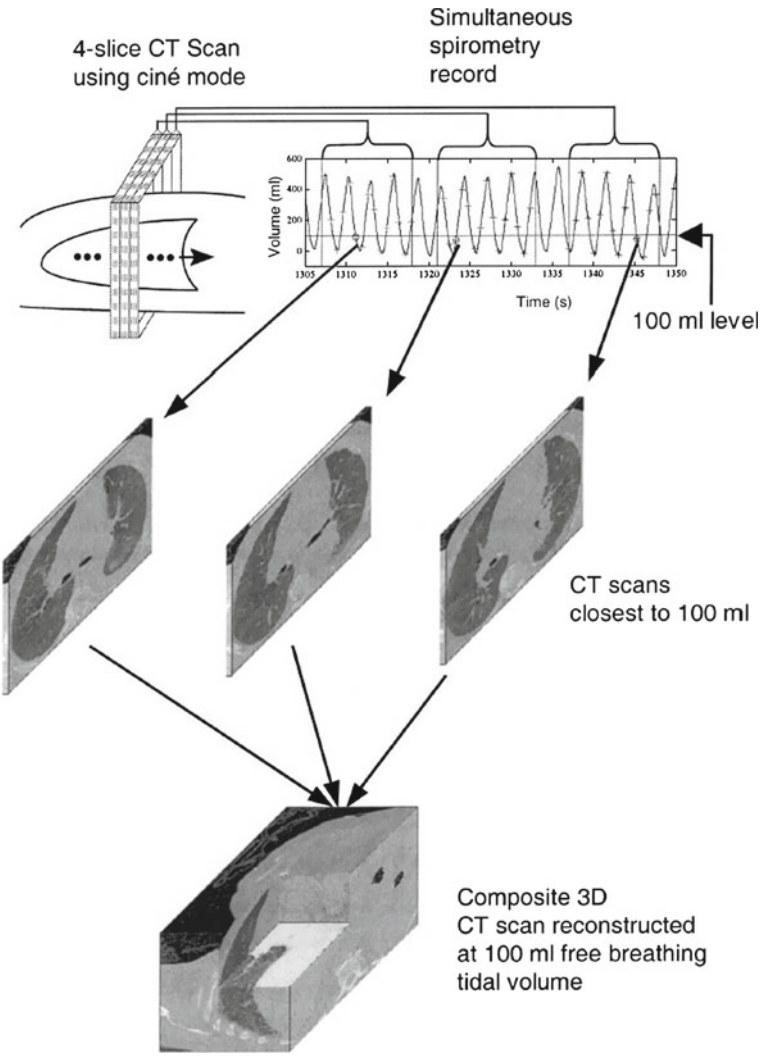


**Fig. 3.2** Process for building a 3D CT scan from sequentially acquired ciné CT image datasets. In each couch position, a number of ciné images are acquired. The image is from Low et al. [5]

4D CT scans. The scans are acquired at the same time as a breathing surrogate is measured. The breathing cycles are divided in phases that are equal in time between inhalations. The images acquired in each phase are collected for each table position to form single-phase CT images, similar to what is done in Fig. 3.2 for breathing amplitude gating.

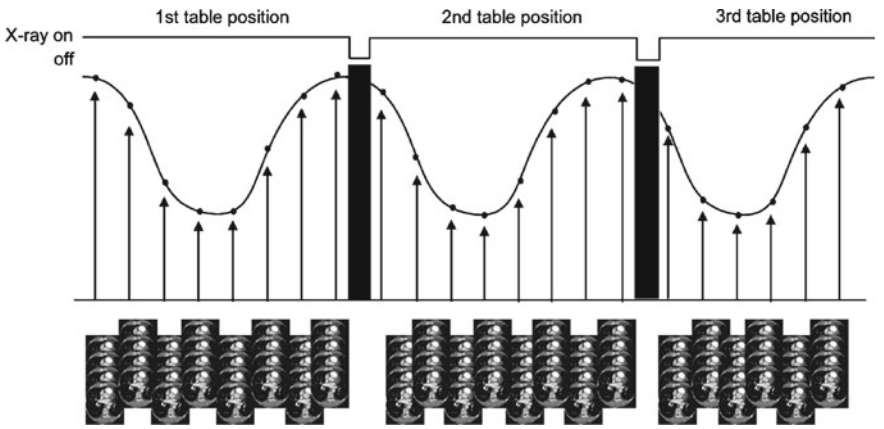


**Fig. 3.3** Phase-based reconstruction of 4D CT scans using a commercial phase-based sequence. The figure is from Pan et al. [8]

### *3.3.1 Amplitude and Phase-Angle Sorting*

CT manufacturers have long provided robust cardiac gating acquisition and sorting tools. This is because the cardiac cycle is straightforwardly measurable and temporally stable. Typically, CT scans required well monitoring the cardiac cycle and the x-ray projections are resorted according to the cardiac phase, which is defined as the relative time between equivalent points in the cardiac cycle. Because of the stability of the cardiac cycle, this approach has been extremely successful. Figure 3.4 shows an outstanding surface rendered image of the heart from Wijesekera et al. [11]. In contrast, Fig. 3.5 shows an example of retrospectively phase-based sorted 4D CT acquired using a ciné protocol [4]. Artifacts are present at the dome of the diaphragm and tumor volume and shape (below the cross-hairs in each of the four images) are altered from phase to phase making it difficult to delineate correctly. Such artifacts are common because breathing is less reproducible than cardiac motion, and both approaches to sorting respiratory-gated CT scans are affected from this motion variability.

#### 3.3.1.1 Phase-Angle Sorting

In phase-angle gating, the breathing cycle is assumed to be reproducible in time; each breath is assumed to have the same characteristics as other breaths. A specific phase is selected as the start of respiration. The time between then and the time at which that same phase is next reached is a single breathing period. The breathing cycle is subdivided as a fraction of the time between those phases. For example, if the breathing cycle is begun at peak exhalation, and the time to the peak inhalation is

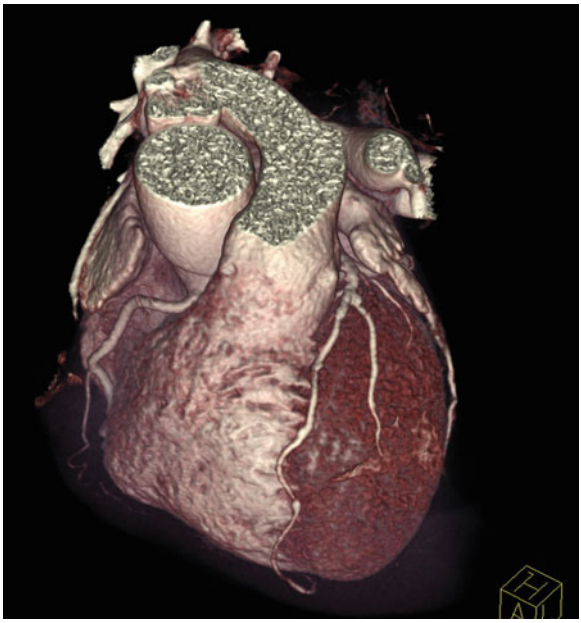

**Fig. 3.4** Surface rendered image of the heart acquired using cardiac gated CT. The figure is from [11].

40 % of the total breathing period, peak inhalation is said to occur at the 40 % phase. Often, phases are described in terms of angles with 360° between successive breaths.

Phase angle sorting is effective for regular breathing patients. The patient's breathing amplitude is consistent, so their internal anatomy will reproducibly located in the same place during the same phase angle. When breathing is irregular, however, the algorithm breaks down. For example, if a deep breath is followed immediately by a shallow breath, the peak inhalation phase will be identified in both breaths and be considered equivalent. The phase angle sorting algorithm will collect image data from both of those breaths at the same phase and include them in an image that is representative of inhalation. Clearly, the internal anatomy will be positioned differently for the deep and shallow breaths. Because of the similarity between phase angle respiratory sorting and cardiac sorting, this algorithm was the first to be commercially implemented because of the significant effort that imaging vendors had already invested in cardiac imaging.

Seppenwolde et al. [9] reported in 2002 their breathing motion model which was based on the phase angle approach. They had reviewed a series of fluoroscopic video images of implanted fiducial markers in a large number of lung cancer patients. The motion of the markers appeared either straight or took an elliptical pattern. They parameterized the motion into components that were aligned to the motion ellipses. Their model provided flexibility such that it could accommodate both straight and elliptical motion. For example, in Fig. 3.6, two examples are shown, one with straight

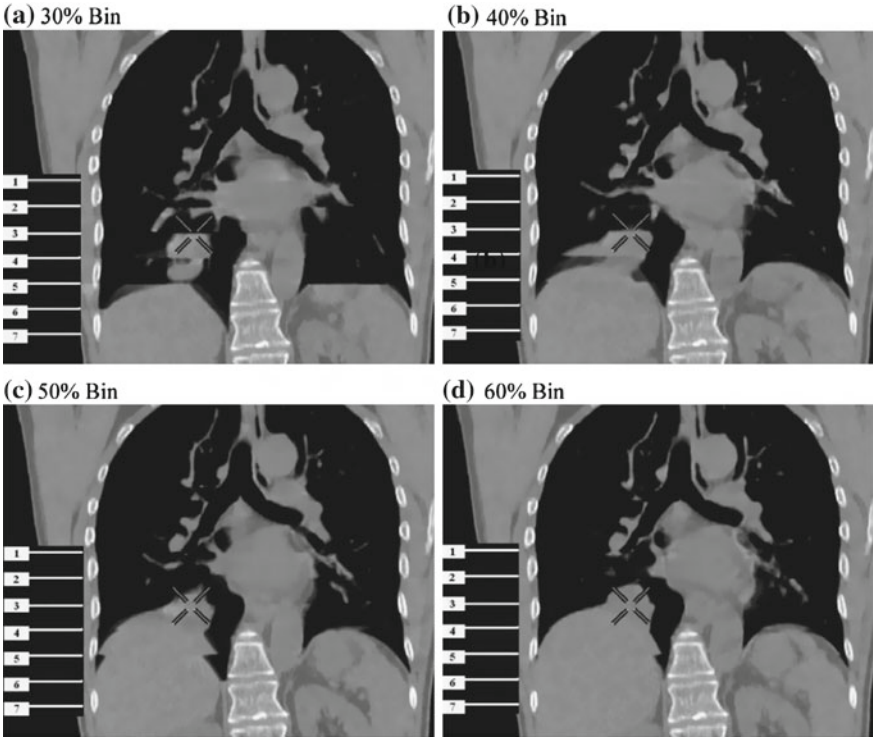


**Fig. 3.5** Examples of artifacts in ciné CT caused by irregular breathing and retrospective sorting (image taken from [4]). The *numbered lines* on each image represent the detector span for different couch positions (2 cm in this case). The cross-hairs provide a common reference point in each image

and one with elliptical motion. As can be seen by the figure, the development of elliptical motion comes from a phase difference between the two directional components. While this technique worked well for regular breathing, it failed to allow the modeler to manage irregular breathing. Figure 3.7 compares modeled motion to measured motion in the craniocaudal direction for two patients. Figure 3.7a represents a regular breather and shows the model was able to accurately describe breathing motion. Figure 3.7b shows an irregular breather, in this case defined as a breathing pattern with a variable frequency. The model, having fixed frequency, phase, and amplitude is unable to manage variations in any of these quantities.

#### 3.3.1.2 Amplitude-Based Sorting

In contrast to phase angle sorting, amplitude-based sorting assumes that internal anatomical positions of tissues are functions of the depth of breathing rather than the fraction of time between successive breaths. Irregularity in breathing amplitude

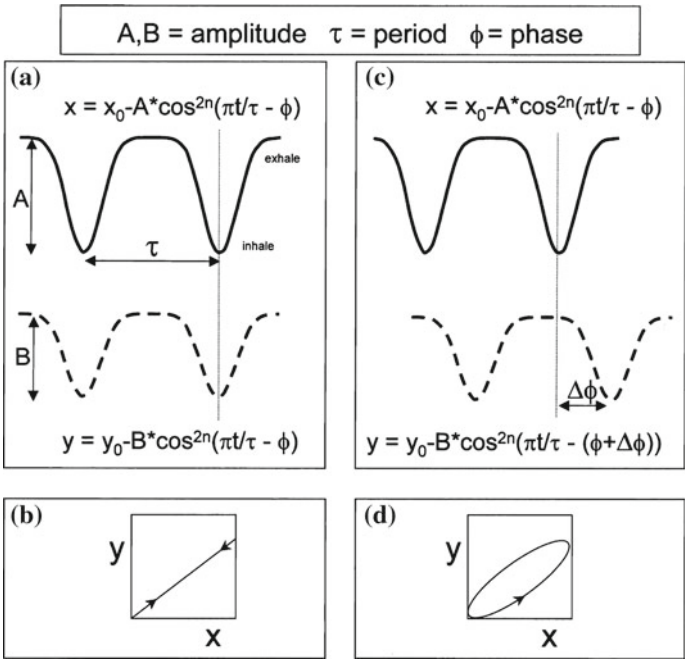


**Fig. 3.6** Breathing tissue motion model proposed by Seppenwolde et al. [9]. The model describes embedded radiopaque marker locations as periodic functions in time

or frequency is straightforwardly managed by amplitude sorting. Images acquired during irregular breathing incur fewer artifacts when using amplitude sorting than phase angle sorting. The main issue with amplitude-based sorting is that it does not distinguish between inhaling and exhaling, so that a specific amplitude during mid-inhalation and mid-exhalation will be treated the same. This makes it impossible to model hysteresis motion with strict amplitude-based approaches. However, the greatest component of motion is not due to hysteresis but due to the expansion and contraction of lungs during inhalation and exhalation, respectively.

Lu et al. [6], examined phase angle and amplitude based sorting and its relation to irregular breathing. They reconstructed 3-D image data sets for 12 breathing phases for 40 patients, computing the air content, defined as the integrated amount of air in the lungs based on the CT scan and using air content as a surrogate for tumor position. They correlated breathing phase and amplitude to air content and determined the correlation residual. In most cases, amplitude sorting resulted in a smaller residual than phase angle sorting. When tidal volume was used as the comparator, the variation was always less for amplitude than phase angle gating. Figure 3.1 shows an example from Lu et al. [6] that explains the differences between amplitude and phase-angle sorting for an irregular breathing patient. The times that are consistent with a specific part of the breathing cycle, in this case the definition of mid-inspiration, are

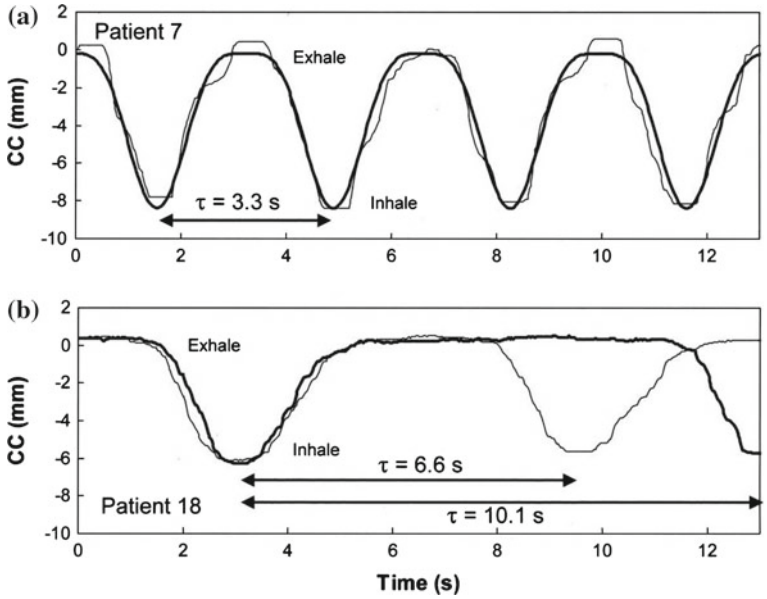


**Fig. 3.7** Example of breathing motion model results from Seppenwoolde et al. [9] for (**a**) a regular-breathing patient and (**b**) irregular breathing patient (defined here as a patient with a variable breathing period). The model works well when the breathing frequency, amplitude, and phase are stable, but breaks down if any of these three factors change

highlighted in the figure. The selected times correspond to the point in time where projection data would be used to reconstruct a mid-inspiration image. In the amplitude sorted case (Fig. 3.1a), those points in time are identified when the patient's tidal volume was between 250 and 450 mL. In contrast, Fig. 3.1b shows mid-inspiration times when phase-based sorting is used. In this example, mid-inspiration was defined as halfway in time between maximum expiration and maximum inspiration. When examining the amplitudes during these times, times where the phase-based sorting algorithm would select projection data, it is clear that not all of the times correspond to a physiologically reasonable definition of mid-inspiration.

## 3.4 Challenges with Ciné CT

### *3.4.1 Cone-Beam Artefacts in Ciné CT*

Single slice CT projections can be approximated as being one-dimensional. The finite longitudinal dimension causes volume averaging. Multislice CT scanners, on the other hand have longitudinally diverging beams. The projecting rays of even a

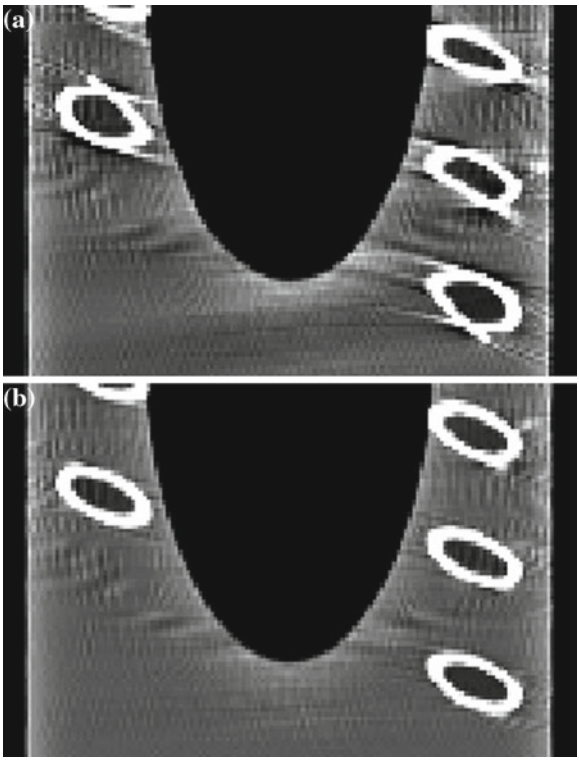


**Fig. 3.8** Example of cone-beam artifacts in multisclice CT scanners. **a** This image was reconstructed using fan-beam reconstruction. **b** This image was reconstructed using cone-beam reconstruction. Images are from Barrett and Keat [1]

4-slice CT scanner are not parallel to the plane of rotation for the first and fourth slice. Images can be reconstructed assuming that the rays for each slice lie in parallel planes and for a 4-slice CT scanner this approximation does not cause significant image artifacts.

As the number of slices increases, and specifically the out-of-plane angle of the rays increases, the images start to contain cone-beam artifacts. Figure 3.8 shows an example of scans of a chest phantom acquired using a 16-slice CT scanner [1]. Figure 3.8a, b were reconstructed using fan-beam reconstruction and cone-beam reconstruction, respectively. The chest phantom includes synthesized ribs that provide high contrast surfaces with which to evaluate the artifacts. The ribs in the fan-beam reconstructed images contain clear artifacts in spite of the fact that the scanner used to acquire these images was only 16 slice (there are 356 slice scanners available). The artifacts disappear when cone-beam reconstruction is used.

Manufacturers of CT scanners often do not reconstruct ciné images using cone-beam algorithms. Cone-beam algorithms remove the artifacts by using projections that would otherwise be associated with more-off axis slices. This reduces

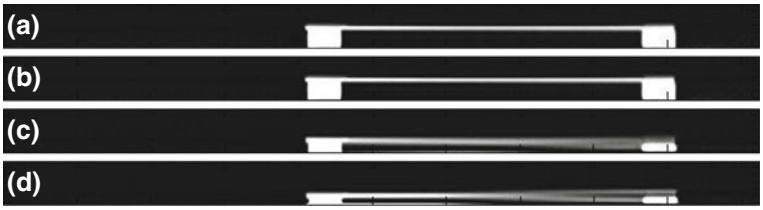


**Fig. 3.9** Coronal CT images of a cylindrical acrylic rod of 3 mm diameter illustrating the blurring and doubling cone-beam CT artifact. The entire 500 mm FOV of the scanner is displayed. **a** Rod placed at Z = 1 mm relative to the center of field of view. **b** Rod placed at Z = 3.6 mm. **c** Rod placed at Z = 6 mm. **d** Rod placed at Z = 8.4 mm

the reconstruction volume such that it is no longer equal to the number of slices multiplied by the slice width. Acquisition of abutting ciné CT volumes would require overlapping of the radiation fields, which manufacturers are reluctant to do. Cone-beam artifacts become worse as the cone-beam angle increases.

An example of the impact of cone beam artifacts is shown in Fig. 3.9. A 3 mm diameter cylindrical acrylic rod was scanned using a 64 slice CT scanner with a 4 cm coverage. The acrylic rod was placed to intercept the central detectors and was oriented in the transverse plane. A single scan was acquired and then the rod was moved and scanned a total of three times, each time at a greater and greater distance from the central axis plane. When the rod was placed near the edge of the field of view in both the axial (8.4 mm) and longitudinal directions, the image of the rod was split by at least 5 mm. This implies that soft tissue structures such as vessels, bronchial branches, and nodules would exhibit similar splitting near the field edge. Figure 3.10 shows intensity profiles taken in a longitudinal direction through the images of the acrylic rod when the rod was 8.4 mm from the central plane. The profiles are identified by their distance from the central axis. The variation in the imaged shape of the cylindrical rod is evident in the profiles. When the rod is near the CT scanner central axis, the profile is nearly Gaussian in shape. At approximately 8 cm from central axis and extending to the edge of the field, the shape of the profile changes from a single peak to a double peak, consistent with the image shown in Fig. 3.9d.

The cone-beam artifacts do not appear to affect clinical use of lung CT scans. The structures that are impacted are the small vessels and bronchi, which are typically not the subject of contouring or segmentation. Motion artifacts are usually present in these CT scans and some of the cone-beam artifacts may have been misinterpreted as motion artifacts. The challenge with having these artifacts present in the images comes when the images are being used with automated segmentation. Systematic artifacts that make the tissues appear differently depending on which detector row they intersect will make registration difficult because the registration algorithms expect the structures to have consistent shapes no matter where they are imaged.

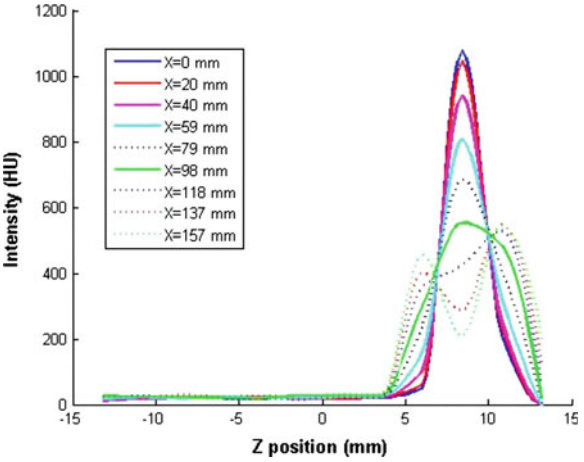


**Fig. 3.10** Longitudinal profiles of the image of the acrylic rod at various sagittal slices (as indicated in the legend). The rod was placed horizontally in an axial plane Z = 8.4 mm relative to the center of the FOV. The profiles have been interpolated from the raw pixel values using cubic interpolation

### *3.4.2 Abutment Challenges*

An important step in developing breathing models is mapping the breathing motion. Ciné CT scans have the advantage that the time of acquisition is accurately known so the specific breathing phase associated with the scan data can also be accurately determined. This allows researchers in breathing motion modeling to assign breathing phases. However, in all cases, some form of image registration is required to map the motion of the lung tumor or normal lung to provide the raw data for a breathing model.

Tissue registration, specifically deformable image registration is challenging for ciné CT acquired image data. If the user intends to build a volumetric CT at a specific breathing phase, misregistration artifacts will occur at the abutment regions between neighboring ciné acquisitions. These are caused by the use of images that were acquired at slightly different breathing phases so the lung tissues do not match exactly at the abutments. Image registration algorithms are ill-suited to manage such tissue discontinuities. One way of managing this is to deformable register images to a common breathing phase and then stack them to form a single volumetric image dataset that corresponds to that phase. This was proposed by Ehrhardt et al. [2]. They used tidal volume as the method of describing the breathing cycle and interpolated pairs of ciné images to a selected tidal volume. The two sets of ciné images that were closest to the desired tidal volume, one larger and one smaller, were used. The full image registration using optical flow defined motion vectors between images and the resulting image was interpolated to the appropriate tidal volume. Figure 3.11 shows an example of the interpolation process. The diaphragm dome shows the amount of

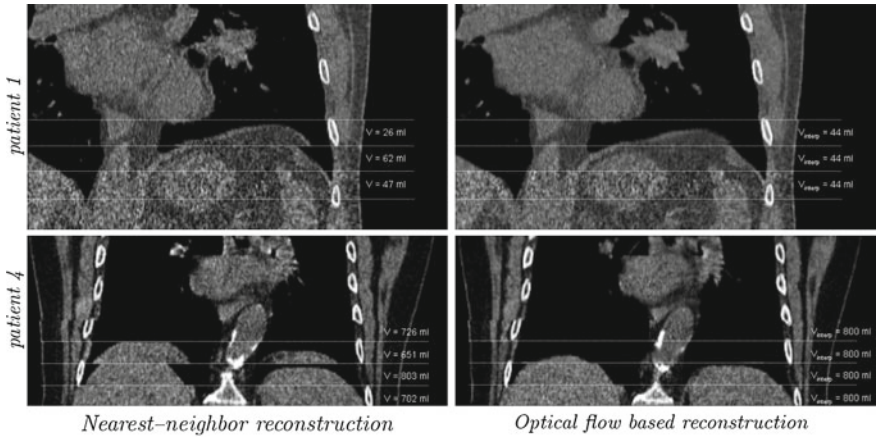


**Fig. 3.11** Examples of the impact of interpolating to a common breathing phase (in this case 44 and 800 ml tidal volumes) on the image abutment quality for ciné CT scanning. Figure from Ehrhardt et al. [2].

misregistration when nearest neighbor tidal volumes are used. Using optical flow interpolation the misregistration artifact becomes much smaller.

## 3.5 Future of Respiratory Sorting

Even when employing amplitude-based sorting, and managing the variation in breathing amplitude, the breathing amplitude variations still have an impact in the quality of the resulting CT scans as well as the interpretation of the scans. For example, as shown in Fig. 3.1, there is a single breath near the time point of 545 s that is deeper than the remaining breaths. The internal lung tissues presumably moved to locations that differed from the rest of the breaths shown in Fig. 3.1. Treatment plans conducted using amplitude-based sorting would not likely have the feedback to know that the patient takes an occasional deep breath. Therefore, some feedback to provide the planner with an understanding of motion outside of that which is provided by the images would be extremely useful.

Figure 3.12 shows the breathing pattern for a regular breathing patient as well as a differential histogram that shows the relative time that the patient spent at each amplitude. The breathing histogram can be used firstly to identify meaningful definitions of peak inhalation and exhalation. Rather than select the two points in time that have the maximum and minimum breathing extent, a more useful definition would be based on the ability to generate an amplitude based CT scan with only minor artifacts. The minimum amplitude for which a useful CT scan can be constructed is typically the 5th percentile. Similarly, an amplitude for which a CT scan can reliably be constructed at inhalation is often the 85th percentile. The histogram shows both

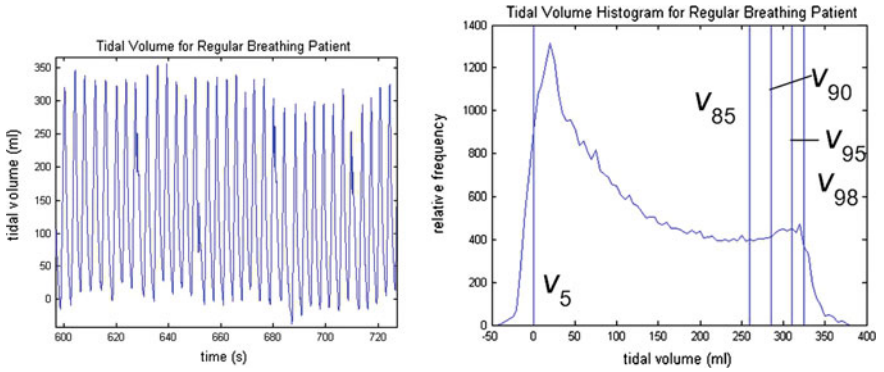


**Fig. 3.12** **a** Breathing pattern for a regularly breathing patient. **b** The histogram corresponding to the breathing pattern shown in **a**. The tidal volume percentiles are shown for reference

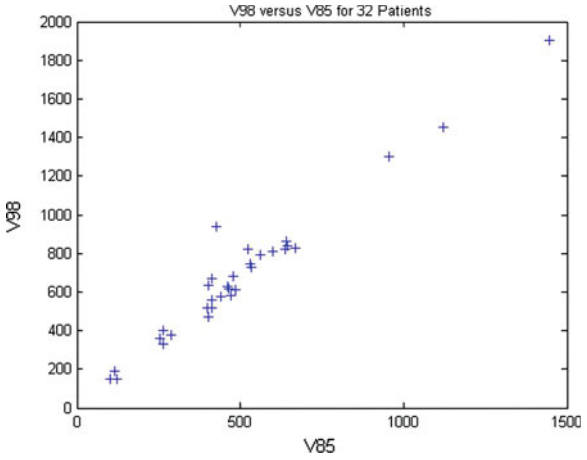


**Fig. 3.13** Comparison of two tidal volumes that could correspond to inhalation for a cohort of 32 patients. $V_{85}$, is often the tidal volume whereby a reliable CT scan can be reconstructed while $V_{98}$ is useful as a metric for deeper inhalation. Linear regression shows that the relationship between the two is $1.39 \pm 0.19$

of these values. However, constructing images at the fifth and 85th percentiles to signify exhalation and inhalation, respectively, ignores the 20 % of time that the patient spends outside of those amplitudes. Therefore, the treatment planner is unaware of how much they should extrapolate the motion they see on the reconstructed CT scans to encompass more of the actual motion envelope.

Figure 3.13 shows the relationship between the 98th percentile and the 85th percentile (relative to the 5th percentile) for 32 patients. The relationship is remarkably linear and has a slope of $1.39 \pm 0.19$. The difference between the 98th percentile and 85th percentile is obviously 13 %, which means that a breathing motion envelope generated using the 85th percentile image should be extrapolated by 40 % in order to

expand the fraction of time that the envelope represents from 80 to 93 %. This type of information would be extremely useful for treatment planners to allow them to more accurately understand the impact of gating decisions as well as the development of internal target volumes to encompass tumors. At this point in time, while the data necessary to provide this information to treatment planners is readily available from the 4DCT acquisition, it is neither analyzed nor provided.

## References

1. Barrett, J.F., Keat, N.: Artifacts in CT: recognition and avoidance. Radiographics **24**(6), 1679–1691 (2004)
2. Ehrhardt, J., Werner, R., Säring, D., Frenzel, T., Lu, W., Low, D., Handels, H.: An optical flow based method for improved reconstruction of 4D CT data sets acquired during free breathing. Med Phys **34**(2), 711–721 (2007)
3. Ford, E.C., Mageras, G.S., Yorke, E., Ling, C.C.: Respiration-correlated spiral CT: a method of measuring respiratory-induced anatomic motion for radiation treatment planning. Med Phys **30**(1), 88–97 (2003)
4. Langner, U.W., Keall, P.J.: Prospective displacement and velocity-based cine 4D CT. Med Phys **35**(10), 4501–4512 (2008)
5. Low, D.A., Nystrom, M., Kalinin, E., Parikh, P., Dempsey, J.F., Bradley, J.D., Mutic, S., Wahab, S.H., Islam, T., Christensen, G., Politte, D.G., Whiting, B.R.: A method for the reconstruction of four-dimensional synchronized CT scans acquired during free breathing. Med Phys **30**(6), 1254–1263 (2003)
6. Lu, W., Parikh, P.J., Hubenschmidt, J.P., Bradley, J.D., Low, D.A.: A comparison between amplitude sorting and phase-angle sorting using external respiratory measurements for 4D CT. Med Phys **33**(8), 2964–2974 (2006)
7. Pan, T.: Comparison of helical and cine acquisitions for 4D-CTimaging with multislice ct. Med Phys **32**(2), 627–34 (2005)
8. Pan, T., Lee, T.Y., Rietzel, E., Chen, G.T.Y.: 4D-CT imaging of a volume influenced by respiratory motion on multi-slice ct. Med Phys **31**(2), 333–40 (2004)
9. Seppenwoolde, Y., Shirato, H., Kitamura, K., Shimizu, S., vanHerk, M., Lebesque, J.V., Miyasaka, K.: Precise and real-time measurement of 3D tumor motion in lung due to breathing and heartbeat, measured during radiotherapy. Int J Radiat Oncol Biol Phys **53**(4), 822–834 (2002)
10. Underberg, R.W.M., Lagerwaard, F.J., Cuijpers, J.P., Slotman, B.J., van Sörnsen de Koste, J.R., Senan, S.: Four-dimensional CT scans for treatment planning in stereotactic radiotherapy for stage I lung cancer. Int J Radiat Oncol Biol Phys **60**(4), 1283–1290 (2004)
11. Wijesekera, N.T., Duncan, M.K., Padley, S.P.G.: X-ray computed tomography of the heart. Br Med Bull **93**, 49–67 (2010)